Korean J. Chem. Eng., 38(3), 485-497 (2021)
DOI: 10.1007/s11814-020-0718-8

pISSN: 0256-1115
eISSN: 1975-7220

Degradation mechanism, reaction pathways and kinetics for the mineralization of Bisphenol A using hybrid ZnO/graphene oxide nano-catalysts

Renuka Garg, Renu Gupta, and Ajay Bansal†

Department of Chemical Engineering, Dr B R Ambedkar National Institute of Technology, Jalandhar, Punjab-144011, India
(*Received 9 July 2020 • Revised 17 November 2020 • Accepted 22 November 2020*)

Abstract−Removal of Bisphenol A (BPA) from surface waters is necessary before consumption. A study, therefore, was conducted to degrade BPA using graphene oxide, ZnO and ZnO decorated on graphene oxide. Hydrothermal method was used to synthesize the hybrid nano-catalysts. 99.5% photocatalytic degradation of BPA was achieved by using $ZG_{0.6}$ nano-catalyst in comparison to bare ZnO and GO nano-catalysts at natural pH of 7.5 in 60 min of UV irradiation. The higher photocatalytic activity of $ZG_{0.6}$ nano-catalyst could be ascribed to an improved surface area, efficient charge separation as well as the decreased recombination rate of electron-hole charge carriers, leading to the generation of highly reactive hydroxyl radicals for the degradation of BPA. Photocatalytic degradation followed Langmuir-Hinshelwood model with pseudo-first-order kinetics. The degradation mechanism is also detailed with identification of reaction intermediates. Degradation pathways, based on LCMS analysis, have been proposed. The pathways revealed the formation of smaller by-products such as phenol, hydroquinol and (Z)-3-hydroxyacrylaldehyde. The developed $ZG_{0.6}$ nano-catalyst were found to be reusable for consecutive five runs without much loss in the activity and have the advantage of effective charge separation.

Keywords: Bisphenol A, Hybrid Nano-catalyst, Photocatalytic Degradation, Degradation Pathways

INTRODUCTION

Water pollution has emerged as a major threat to human as well as aquatic life due to continuous discharge of untreated refractory pollutants such as pharmaceuticals, dyes, pesticides and industrial effluent into water bodies. BPA, i.e. 2,2-bis(4-hydroxyphenyl) propane, is extensively used as a monomer and an intermediate in production of polycarbonates, polyesters, plasticizers, pesticides and epoxy resins [1]. About 95% of BPA is used in production of plastics such as polycarbonate resins and epoxy resins [2,3]. It is employed as a phenolic developer in paper industries, as an antioxidant to produce polyvinyl chloride plastics and also finds applications in daily life products, such as water bottles, food cans, baby feeding bottles, electronic goods, dental sealing, plastic containers and epoxy glues [4]. With an estimated production of 6 billion pounds per year BPA is one of the most produced synthetic chemicals [5]. BPA is commonly found in wastewater and finds its way into water bodies through effluents of industries, landfill leachate, sewage treatment plants and degradation of plastic coatings of drinking water pipelines [6]. BPA has a tendency to leach out into groundwater owing to its moderately high solubility from 120 to 300 mg/L in water. Bisphenol A (BPA) is an endocrine disruptor with the reported concentration ~0.15-30 mg/L in surface waters [7,8] and 6.5 ng/L in drinking water [9].

Continuous exposure to BPA is reported to cause diabetes, infertility, birth defects, heart disease, cancer, disturbed reproductive and hormonal activities in humans [10]. The reported studies reflect that even low concentrations (μg/L) of BPA have harmful effects on aquatic organisms such as morphological deformities, hemorrhage, embryonic deformities and inhibit ovulation [5].

The European Commission has classified BPA as "moderately toxic" compound to aquatic biota [5]. In 2015, European Food Safety Authority decreased the acceptable daily intake to 4 μg/kg bw/day from the 50 μg/kg bw/day to improve the hazardous health effects due to BPA [11]. Hence, it becomes necessary that wastewaters having significant concentrations of BPA be treated effectively before human consumption.

To eradicate refractory organic compounds from water, heterogeneous photocatalysis can provide an efficient, eco-friendly and cost-effective solution. It also has the advantage of complete oxidation of organic pollutants with no formation of sludge. Further, zinc oxide (ZnO) is usually a preferred choice for photocatalysis owing to its fascinating properties. At the same time, ZnO has the limitation of the faster recombination rate of electron and hole pairs, which reduces the photocatalytic activity [12]. Hence, to overcome this limitation it can be coupled with other semiconductors and carbonaceous materials. Herein, graphene oxide (GO) can be used as a decorating material for boosting the photocatalytic activity of ZnO due to its high surface area, high electron conductivity and efficient charge separation capabilities [13]. Previously, ZnO/GO nanocomposites were synthesized by various techniques and their photocatalytic activity towards organic pollutants was studied by several researchers. Jain et al. [13] studied the catalytic performance of ZnO/GO nanocomposites against brilliant green dye with 85.71% degradation after 120 min at 6 pH. Nguyen et al. [14] achieved 95% degradation of methyl orange over ZnO/GO nanocompos-

†To whom correspondence should be addressed.
E-mail: bansala@nitj.ac.in
Copyright by The Korean Institute of Chemical Engineers.

ites. Maruthupandy et al. [15] studied degradation of Rhodamine-B, methylene blue and methyl orange dyes over ZnO/GO nanocomposites, whereas Durmus et al. [16] applied this composite for basic Fuchsin dye. Considering the reported studies, it was observed that the combination of ZnO and GO shows better photocatalytic activity towards refractory organics like dyes. However, the degradation of BPA using ZnO/GO photocatalyst could not be traced in the literature. Therefore, it is worthwhile to extend and explore GO based ZnO nano-photo-catalysts for degradation of BPA.

Some of the studies are reported for BPA removal from aqueous systems, such as adsorption [17,18], sonication assisted Fenton and photo-Fenton process [1,19]. Al-Kahtani et al. [10] observed 88% degradation of BPA using ZnS/NSDC photocatalyst at alkaline conditions (pH 9) for 150 min, whereas, Hak et al. [20] found highest degradation in the acidic medium at pH 3. Ozmen et al. [21] observed 95% degradation using Mn-doped TiO_2 after 4 h. Further, Bechambi et al. [22] observed complete BPA degradation and 70% mineralization using C-doped ZnO/H_2O_2 at pH 8, but relatively at very high irradiation time of 24 h. Carefully reviewing the literature, it was observed that these studies had one or more limitation in terms of very high or very low pH (making it difficult to discharge in natural water bodies without any further treatment) and large time for degradation (resulting in high processing cost).

With the intent to overcome these limitations, the present study was carried out with a focus on higher degradation, near to neutral process conditions, reduced degradation time and synthesis of effective photocatalyst. ZnO decorated graphene oxide nanocomposites were synthesized by simple hydrothermal route and systematic investigations were made to characterize the prepared catalysts. Further, LC-MS study was also carried out to identify the reaction intermediates. Based on the study reaction intermediates, reaction mechanism and degradation pathways have been proposed.

MATERIALS AND METHOD

Graphite powder (98%) was obtained from Loba Chemie, India. Bisphenol A, zinc acetate dihydrate, HCL (37%), H_2SO_4 (98%), $KMnO_4$ were procured from Sigma Aldrich. Sodium citrate, sodium hydroxide and ethanol were purchased from S.D. Fine Chemicals Limited, India. De-ionized water was used for the preparation of all solutions.

1. Synthesis of ZnO/GO Nanocomposite

Graphene oxide (GO) was synthesized using modified Hummers method [23]. Xu et al. [24], synthesized ZnO nanoflowers via hydrothermal route. This recipe was used to synthesize ZnO nanorods. Recipe due to Xu et al. [24], was extended to synthesize ZnO/GO nanocomposites by additionally adding graphene oxide to the reaction mixture. In brief, equimolar ratio (2.5 mmol) of sodium citrate and zinc acetate dihydrate was dissolved in 50 mL deionized water. Then 12 mL of sodium hydroxide was added dropwise into the above solution. GO suspension was added slowly in above mixture under vigorous stirring. The reaction content was then subjected to sonication for 15 min. The mixture was transferred into hydrothermal autoclave. The temperature of the hydrothermal autoclave was maintained at 120 °C and the mixture was kept for 5 h. The mixture was filtered and grey colored precipitates were obtained. The precipitates were washed several times using deionized water and dried at 60 °C. $ZG_{0.3}$, $ZG_{0.6}$ and $ZG_{0.8}$ nanocomposites of ZnO/GO nanocatalysts were synthesized by varying the wt% of GO as 0.3 wt%, 0.6 wt% and 0.8 wt%, respectively.

2. Characterization

To characterize ZnO, GO nanocatalysts and to investigate the decoration of ZnO nanorods on graphene oxide, UV-Vis spectra, X-ray diffraction (XRD), field emission scanning electron microscopy (FESEM), energy-dispersive X-ray spectroscopy (EDS), photoluminescence (PL), Brunauer-Emmett-Teller (BET), zeta potential analysis were carried out. The reflectance absorption spectra (DRS) were recorded in the range of 200-900 nm on a double beam UV-Vis spectrophotometer (Model: UV-2600, Shimadzu, Japan) to estimate the band gap of the catalysts. XRD analysis of the catalysts was performed using PAN analytical X-pert PRO spectrometer with Cu-Kα radiation operating at 40 mA and 45 kV in the 2θ range of 10-80°. The samples were analyzed in dried, powdered form. FE-SEM (Nova Nano 450 FEI) was used to investigate the surface morphology of the synthesized nano-catalysts. Energy-dispersive X-ray spectroscopy (EDS) studies were made at 200 kV to determine catalyst elemental composition. Brunauer-Emmett-Teller (BET) surface area was measured by NOVA touch 2LX equipment. The nitrogen adsorption-desorption isotherms were obtained at liquid nitrogen temperature of 77 K after degassing the samples at 180 °C for 3 hrs. Photoluminescence (PL) spectra were recorded on fluorescence spectrometer (Perkin Elmer LS6500) using a Xe lamp (excitation wavelength 300 nm) as light source. Zeta potential analysis of nano-catalysts was recorded by varying the pH of solution using Malvern Zetasizer Nano ZS90. For this purpose, 3 mg of nanocatalysts was dispersed in 30 mL of deionized water before measurement and sonicated for 5 minutes to ensure uniform suspension.

3. Analytical Methods

Total organic carbon (TOC) of the samples was analyzed using the TOC analyzer (ASI-V and TOC-V_{CPN}, Shimadzu, Japan). The non-dispersive infrared method was employed for the detection of TOC. Liquid chromatography-mass spectroscopy (LCMS) analysis was carried out using C_{18} column having 100 mm length and 2.1 mm inner diameter (Q-TOF micro waters, Waters, USA) to determine the masses of the intermediates formed during reaction. The mixture of acetonitrile and water (60 : 40 v/v) was used as the mobile phase with the flow rate of 0.8 mL min^{-1} at 25 °C. The samples were analyzed by electrospray ionization (ESI) in negative mode over the mass range of 50-300 amu before degradation and after the degradation of BPA.

4. Experimental Procedure

The degradation study of BPA (50 ml of 20 mg L^{-1}) was conducted in photocatalytic chamber lined up with galvanized aluminum sheets of dimensions 59 cm×28.5 cm×56 cm. The reactor consisted of $UVC_{254\,nm}$ tubes (model F15T8/GL). The intensity of UV light was measured using UV Power Puck II radiometer (EIT, Inc. Sterling, VA, 20164 USA).

While working with large surface area nano-photo-catalysts adsorption cannot be ruled out. To examine the extent of adsorption, the preliminary study was carried out in the dark without light to quantify BPA removal due to adsorption. The pH of the BPA solution was adjusted using 0.1 M hydrochloric acid and 0.1 M sodium

hydroxide solution. Further, the suspension was irradiated under UVC light in the photocatalytic chamber. The temperature of the reaction in the photocatalytic chamber was maintained by the cooling fans. The effect of light intensity, effect of GO loading on ZnO, the dose of the catalyst, pH of BPA solution and initial BPA concentration was investigated on degradation of BPA. The concentration of each sample was measured at the λ_{max} of 276 nm. The degradation % was calculated using following equation.

$$\text{Degradation (\%)} = \left(1 - \frac{C}{C_0}\right) \times 100 \quad (1)$$

where C_0 is initial concentration of BPA at time t=0, C is the concentration of BPA after time t.

RESULTS AND DISCUSSION

1. Catalyst Characterization

1-1. UV-Vis Diffuse Reflectance Analysis

The absorption spectrum and band gap of synthesized nanocatalysts as observed from UV-Vis spectrophotometer are shown in Fig. 1(A) and (B), respectively. The absorption peak of GO was observed at 230 nm, whereas the absorption edges of ZnO, $ZG_{0.3}$, $ZG_{0.6}$ and $ZG_{0.8}$ were found at 398 nm, 415 nm, 435 nm and 420 nm, respectively (Fig. 1(a)). The corresponding band gap energies were calculated using Tauc plot as $(\alpha h\nu)^2 = A \times (h\nu - E_g)$ [25]. The band gap energy for pure GO, ZnO and $ZG_{0.3}$, $ZG_{0.6}$ and $ZG_{0.8}$ nanocatalysts was found to be 2.1 eV, 3.02 eV and 2.89 eV, 2.60 eV and 2.95 eV, respectively (Fig. 1(b)). The results revealed that incorporation of GO in ZnO reduced the band gap of composites in comparison to ZnO, leading to better photocatalytic activity by utilizing more photon energy to generate electron-hole pairs [26]. The results are in line with study due to Jain et al. [13].

1-2. XRD

The XRD patterns of GO, ZnO, $ZG_{0.3}$, $ZG_{0.6}$ and $ZG_{0.8}$ hybrid nanocatalysts are shown in Fig. 2. The XRD analysis of graphene oxide showed the major diffraction peak at 2θ values of 10.1°, whereas for ZnO the diffraction peaks were observed at 2θ values of 31.0°, 34.4°, 36.1°, 47.2°, 56.5°, 62.7°, 67.9° and 76.9°. However

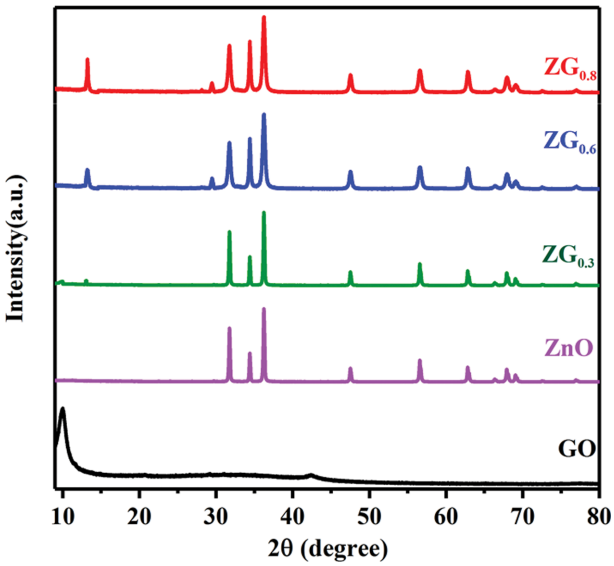


Fig. 2. XRD patterns of GO, ZnO, $ZG_{0.3}$, $ZG_{0.6}$ and $ZG_{0.8}$ nanocatalysts.

the major diffraction peaks for $ZG_{0.3}$, $ZG_{0.6}$ and $ZG_{0.8}$ at 2θ values were 13.1°, 29.7°, 31.0°, 34.4°, 36.1°, 47.2°, 56.5°, 62.7°, 67.9° and 76.9°. The additional peak at 29.7° in ZnO/GO composites was attributed to reduced graphene oxide after hybridization [27]. The diffraction peaks for hybrid nanocatalyst were similar to the characteristic peaks of ICSD card no. 10-0679. The incorporation of GO and ZnO peaks in $ZG_{0.6}$ nanocatalyst confirmed the formation of ZnO nanorods on GO nanosheets.

1-3. FESEM

FESEM image of graphene oxide revealed the formation of thin layers of GO nanosheets (Fig. 3(a)). The rod-like structure of ZnO is clearly visible (Fig. 3(b)) with an average length of 145 nm and a diameter of 50 nm. Fig. 3(c)-(e), shows the formation of ZnO nanorods over GO nanosheets in $ZG_{0.3}$, $ZG_{0.6}$ and $ZG_{0.8}$ nanocomposites. However, due to low amount of graphene oxide, the sheets are not visible in $ZG_{0.3}$. Further, the average length of nanorods

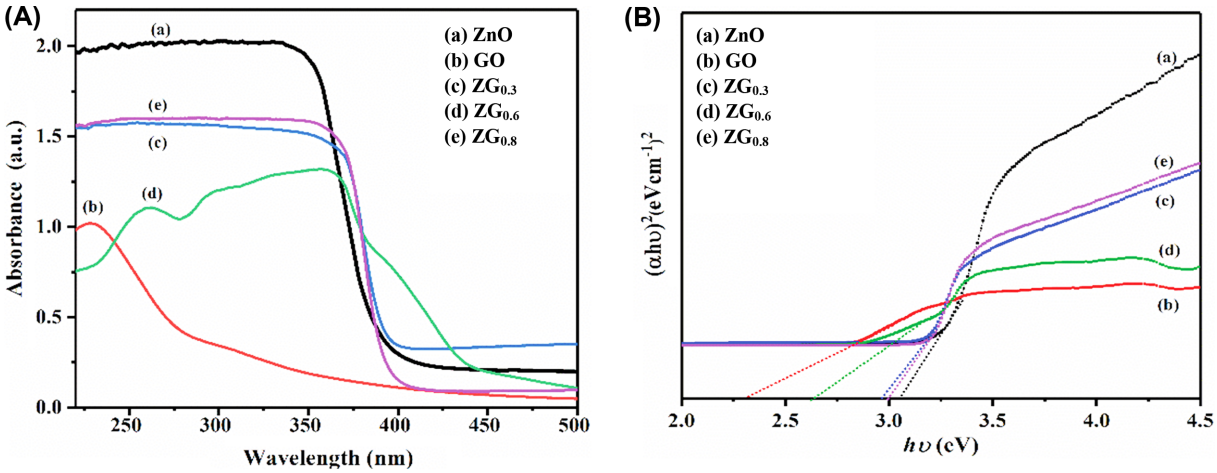


Fig. 1. UV- Vis absorption spectra (A); bandgap energies (B) of GO, ZnO, $ZG_{0.3}$, $ZG_{0.6}$ and $ZG_{0.8}$ nano-catalysts.

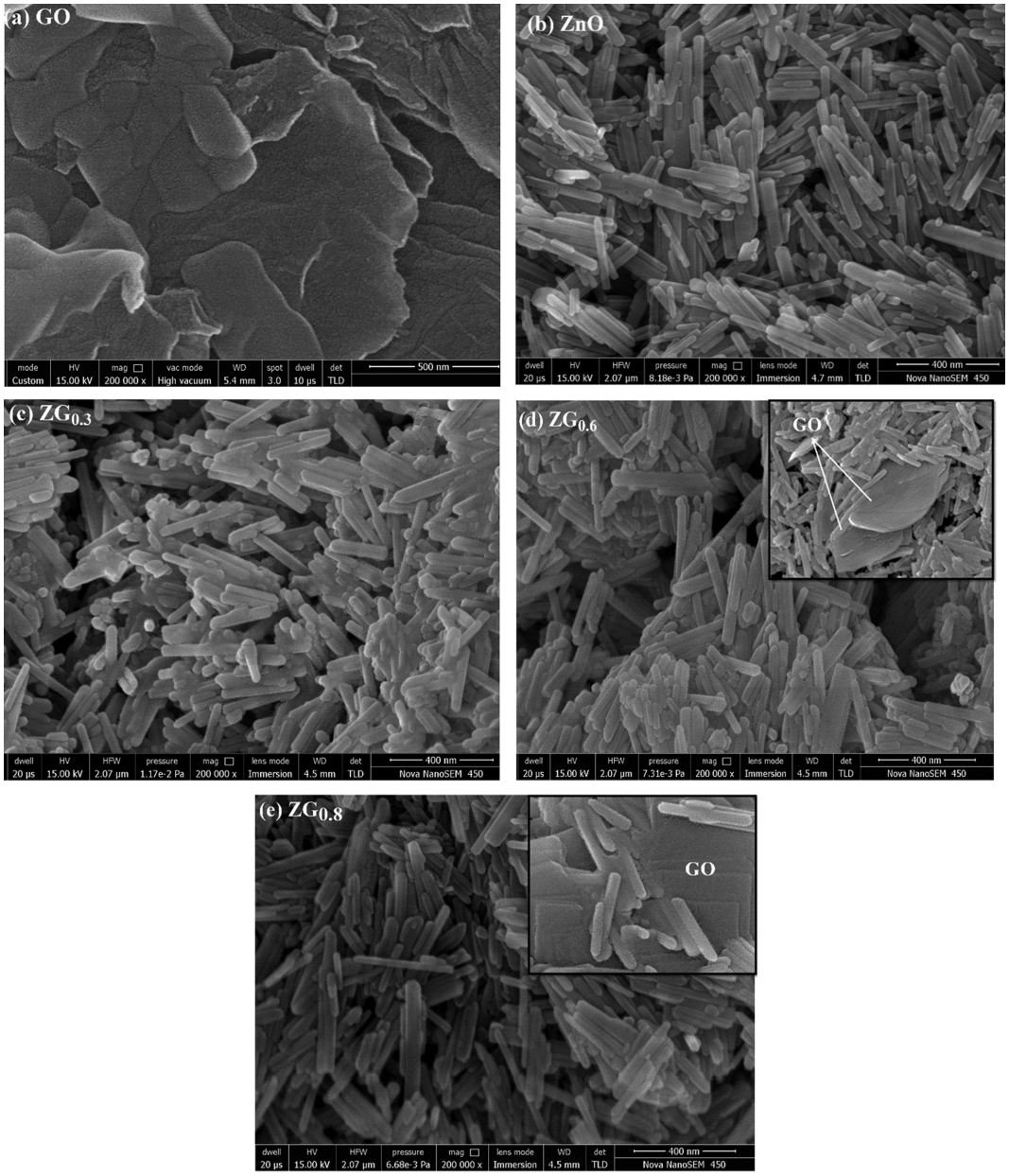


Fig. 3. FESEM images at (200,000x magnification) for GO (a); ZnO (b); $ZG_{0.3}$ (c); $ZG_{0.6}$ (d); $ZG_{0.8}$ (e).

Table 1. Weight % of elements based on EDS spectra

Elements	Atomic wt% ZnO	Atomic wt% GO	Atomic wt% $ZG_{0.3}$	Atomic wt% $ZG_{0.6}$	Atomic wt% $ZG_{0.8}$
Zn	61.6	-	79.0	70.1	60.5
C	-	60.6	11.5	12.7	19.7
O	38.4	39.4	9.5	17.2	19.8

was found in the range of 150-170 nm. The inset of Figs. 3(d) and (e) reveals the dispersion of ZnO nanorods over GO sheets leading to formation of nanocomposites.

1-4. EDS Spectra

The elemental composition and distribution of synthesized nanocomposites were analyzed by energy dispersive X-ray spectroscopy (EDS) and shown in Fig. 4(a)-(e). EDS spectra revealed the presence of elements Zn and O in ZnO catalyst, C and O in GO and Zn, C, and O in $ZG_{0.3}$, $ZG_{0.6}$ and $ZG_{0.8}$ nanocomposites and their compositions are listed in Table 1. It was confirmed from the spectra that there were no elemental impurities in the prepared nano-catalysts.

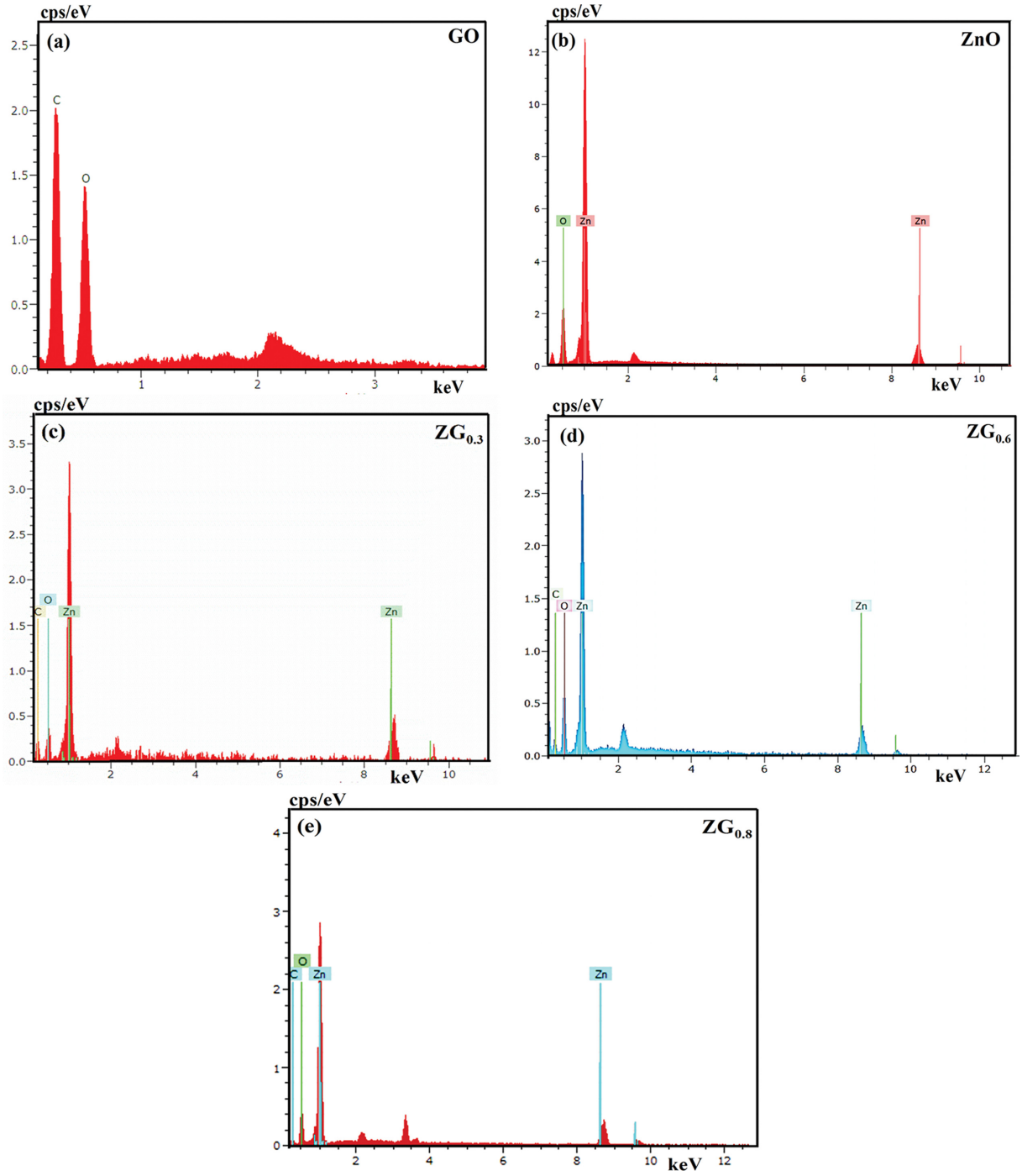


Fig. 4. EDS spectra of GO (a); ZnO (b); $ZG_{0.3}$ (c); $ZG_{0.6}$ (d); $ZG_{0.8}$ (e).

1-5. Photoluminescence Spectra

Fig. 5(a) depicts the PL spectra of ZnO, $ZG_{0.3}$, $ZG_{0.6}$ and $ZG_{0.8}$ nano-catalysts. ZnO/GO nanocomposites showed lower intensities in comparison to ZnO nanorods due to addition of graphene oxide. The lower intensity indicates a reduction in the recombination of generated electron-hole charge carriers for ZnO/GO nano-catalysts, hence effective charge separation. Moreover, GO acts as sink for the electrons transferred from the conduction band of ZnO, enhancing the generation of $^{\bullet}OH$ radicals [15]. Fig. 5(a) reveals the lowest intensity for $ZG_{0.6}$ as compared to $ZG_{0.3}$ and $ZG_{0.8}$ nano-composites.

1-6. BET Surface Area

N_2 adsorption/desorption isotherms for prepared ZnO, $ZG_{0.3}$, $ZG_{0.6}$ and $ZG_{0.8}$ nano-catalysts are shown in Fig. 5(b) and details of specific surface area, pore volume and pore radius of prepared nano-catalysts are given in Table 2. Table 2 reveals that an increase in GO wt% increased the specific surface area and pore volume of $ZG_{0.3}$, $ZG_{0.6}$ and $ZG_{0.8}$ nanocatalysts. However, the pore radius

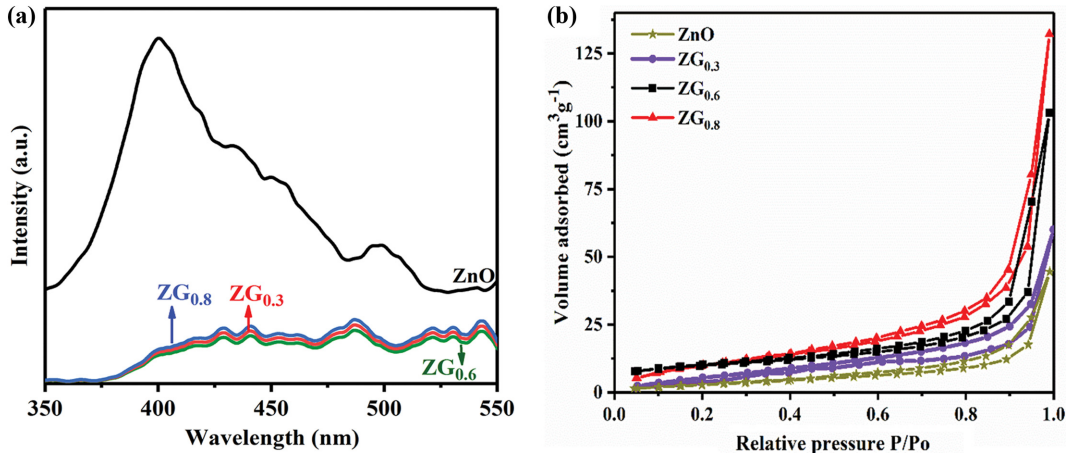


Fig. 5. PL spectra (a); Nitrogen adsorption-desorption isotherms of ZnO, $ZG_{0.3}$, $ZG_{0.6}$ and $ZG_{0.8}$ nano-catalysts (b).

Table 2. BET surface area, pore volume, and pore radius of synthesized nanocatalysts

Samples	BET surface area ($m^2\ g^{-1}$)	Pore volume ($cm^3\ g^{-1}$)	Pore radius (nm)
ZnO	20.1	0.071	1.091
$ZG_{0.3}$	30.5	0.141	0.725
$ZG_{0.6}$	44.5	0.215	0.707
$ZG_{0.8}$	45.7	0.303	0.701

decreased with an increase of GO wt%. The increase in surface area and hence pore volume is attributed to high surface area of graphene oxide (2,630 $m^2\ g^{-1}$) [28].

1-7. Zeta Potential

Zeta potential for GO, ZnO, $ZG_{0.3}$, $ZG_{0.6}$ and $ZG_{0.8}$ was observed to be −39.3 mV, +28.7 mV, −26.2 mV, −35.3 mV and −34.7 mV, respectively (Fig. S1(a); supplementary information). The results indicate that the addition of GO increased the stability of ZnO nanorods in aqueous solutions [29]. Further, zeta potential for $ZG_{0.6}$

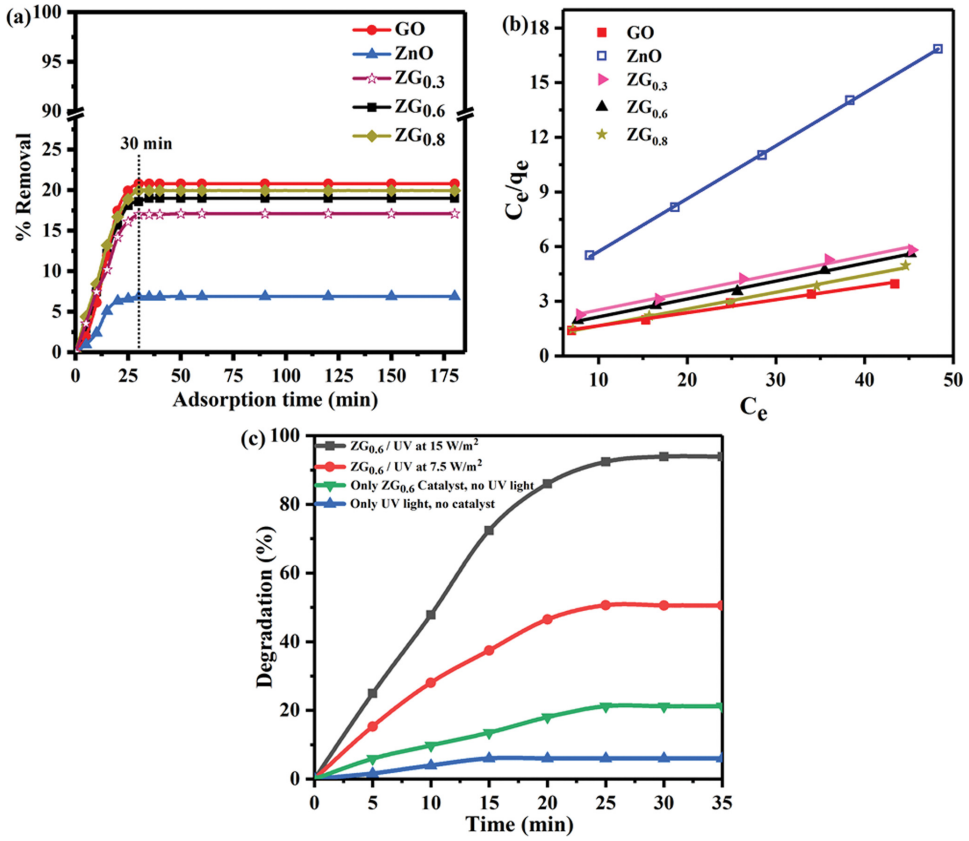


Fig. 6. Adsorption study of BPA (C_o=20 mg L^{-1}, catalyst dose=0.6 g L^{-1}, pH=7.5) (a); Langmuir isotherm for GO, ZnO, $ZG_{0.3}$, $ZG_{0.6}$ and $ZG_{0.8}$ (b); photolytic and photocatalytic study (c).

was recorded by varying the pH of solution to investigate the charge on surface (Fig. S1(b)). It was observed that with increase in pH, zeta potential increased and reached to zero charge at pH 7.0. With further increase in pH it got negatively charged. Archana et al. [30] also reported the point of zero charge of ZnO/GO to be 7.4.

2. Photocatalytic Degradation of BPA

2-1. Adsorption and Photolytic Study

Prior to irradiation, an adsorption study was carried for catalysts with varying concentration of BPA (10-50 mg L^{-1}). It can be clearly seen that for all nanocatalysts, adsorption-desorption equilibrium was reached within 30 min (Fig. 6(a)). Typically, for a concentration of 20 mg L^{-1}, maximum removal of BPA was 19.9%, corresponding to a dose of 0.6 g L^{-1} of $ZG_{0.8}$, whereas maximum removal was 6.5% for ZnO. To quantify the adsorption capacity of nanocatalysts, the experimental data was subjected to the Langmuir-isotherm (Fig. 6(b)). The data is well represented by the Langmuir isotherm, with high regression coefficients, confirming the monolayer adsorption of BPA molecules on catalyst surface. The Langmuir isotherm is expressed by the following equation [30]:

$$\frac{C_e}{q_e} = \frac{C_e}{q_m} + \frac{1}{K_L q_m} \quad (2)$$

where, C_e (mg L^{-1}) and q_e (mg g^{-1}) are the concentration of BPA and adsorption capacity at equilibrium, respectively; q_m (mg g^{-1}) is maximum adsorption capacity of the catalyst; K_L (L mg^{-1}) is the Langmuir constants. Langmuir parameters (q_m and K_L) of isotherms are calculated from the slope and intercept of the linear plot of C_e/q_e Vs. C_e and are summarized in Table 3. The adsorption capacity (q_m) of all the synthesized $ZG_{0.3}$, $ZG_{0.6}$ and $ZG_{0.8}$ nanocomposites was higher in comparison to ZnO nanocatalyst. The higher the GO content, the better the adsorption capacity. It was noticed that an increase in wt% of graphene oxide in ZnO/GO composites led to higher adsorption, which can be attributed to higher surface area of graphene oxide and strong affinity of BPA molecules for catalyst surface [28,31].

A photolytic study of BPA (20 mg L^{-1}) was conducted under exposure of direct UV light without any catalyst, only 3% degradation of BPA was observed (Fig. 6(c)). Further, the photocatalytic degradation study was carried using 0.6 g L^{-1} $ZG_{0.6}$ nanocatalyst in presence of UV light intensity of 7.5 W/m^2 and 15 W/m^2 (measured by UV Power Puck II radiometer, USA). It was observed that degradation of BPA increased from 52.5% to 94.5% with increase in light intensity (Fig. 6(c)). At higher UV intensity, the generation of more hydroxyl radicals enhanced the degradation [32].

Table 3. Parameters of Langmuir isotherm

Catalyst	Slope	Intercept	q_m (mg g^{-1})	K_L (L mg^{-1})	R^2
GO	0.071	0.94	14.08	0.075	0.99
ZnO	0.290	2.82	3.45	0.102	0.99
$ZG_{0.3}$	0.099	1.53	10.10	0.064	0.99
$ZG_{0.6}$	0.098	1.16	10.20	0.084	0.99
$ZG_{0.8}$	0.093	0.73	10.75	0.13	0.99

2-2. Identifying Best Loading of GO in ZnO Nanorods

The effect of loading of GO content on ZnO with varying composition was studied (Fig. 7(a)). It was observed that $ZG_{0.6}$ nanocatalysts exhibited higher photocatalytic activity (99.5%) in comparison to pure ZnO (72.2%) and GO (42.1%) nanocatalysts. By increasing the weight percentage of GO from 0.3 wt% to 0.6 wt%, the photocatalytic activity was increased from 88.1% to 99.5%. This was due to low band gap, improved surface area and decreased recombination rate of charge carriers, which might have boosted the interaction between H_2O/O_2 and electron-hole charge carriers, thus resulting in generation of more hydroxyl radicals [13]. However, raising the GO concentration to 0.8 wt% diminished the degradation to 78.5% attributed to decreased penetration of light [28]. The corresponding rate constant 'k' values were calculated by plotting $\ln(C_0/C)$ vs. t (Fig. 7(b)). It was observed that rate constant 'k' value for $ZG_{0.6}$ nanocatalyst (0.064 min^{-1}) was three times higher than that of ZnO (0.021 min^{-1}) indicating higher photocatalytic activity for the hybrid nanocatalyst.

2-3. Effect of Dosage of $ZG_{0.6}$ Nano-catalyst

The amount of catalyst has a significant effect on degradation of

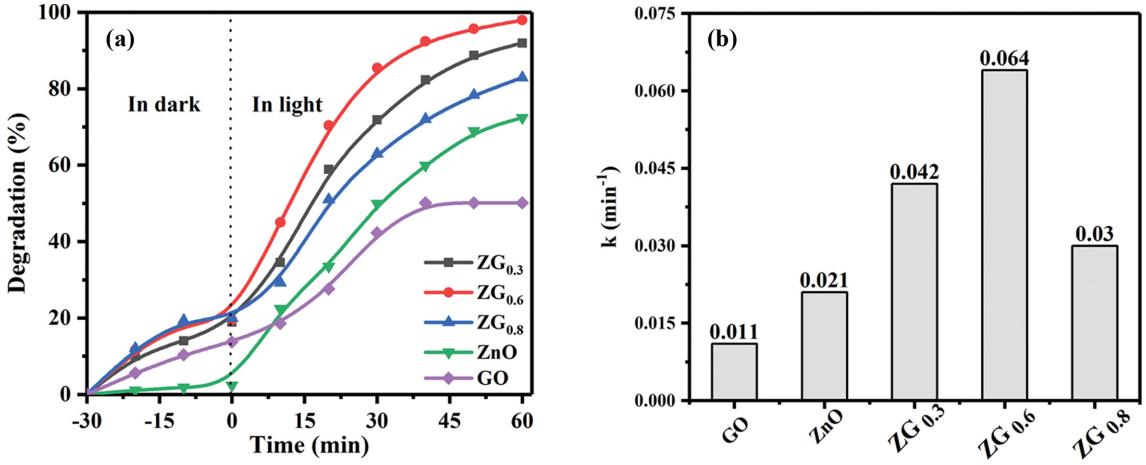


Fig. 7. Effect of loading GO content in ZnO nanorods for photocatalytic degradation of BPA (C_o=20 mg L^{-1}, catalyst dose=0.6 g L^{-1}, pH=7.5, UV intensity=15 W/m^2) (a); Kinetic study for GO, ZnO, $ZG_{0.3}$, $ZG_{0.6}$ and $ZG_{0.8}$ nano-catalysts (b).

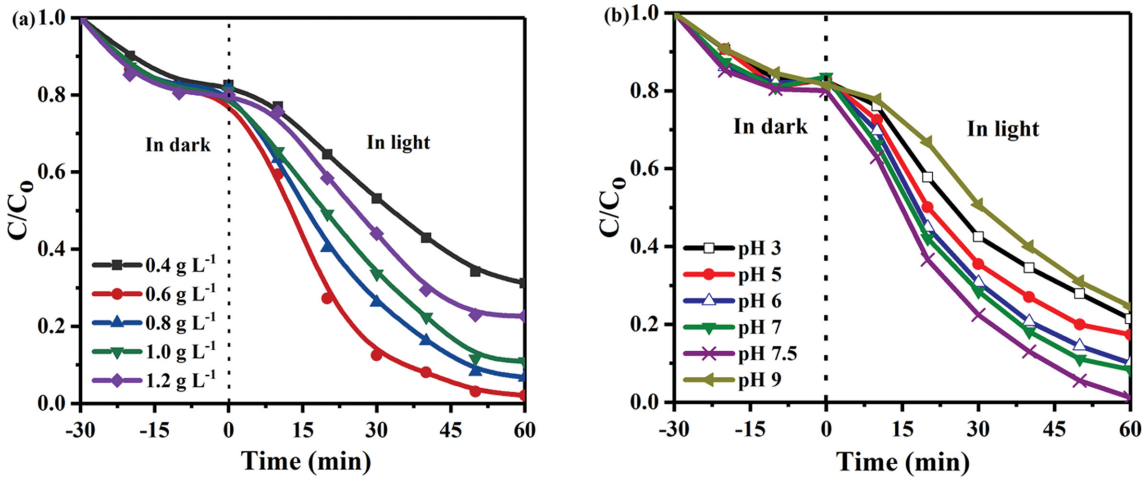


Fig. 8. Effect of dosage of catalyst for photocatalytic degradation of 20 mg L^{-1} BPA using $ZG_{0.6}$ (pH=7.5, UV intensity=15 W/m^2) (a); effect of pH (catalyst dose=0.6 g L^{-1}, UV intensity=15 W/m^2) (b).

BPA. The effect of $ZG_{0.6}$ nanocatalyst was carried out by varying the amount of photocatalyst (0.4 g L^{-1}, 0.6 g L^{-1}, 0.8 g L^{-1}, 1.0 g L^{-1} and 1.2 g L^{-1}). The experiments were carried out at BPA concentration of 20 mg L^{-1} under its natural pH 7.5 for 60 min of UV irradiation. As the catalyst dose was increased from 0.4 g L^{-1} to 0.6 g L^{-1} the degradation was found to increase from 61.1% to 99.5% (Fig. 8(a)). This might be due to an increase in the number of active sites available on the catalyst surface, and as a result, the rate of generation of free radicals (•OH) enhanced, therefore leading to higher degradation of BPA [10,25]. On the contrary, decrease in degradation from 99.5% to 72% was observed as the dose was further increased from 0.6 g L^{-1} to 1.2 g L^{-1} probably due to lesser penetration of light with increased opacity and hence decline in number of active sites, resulting in generation of fewer free radicals [33].

2-4. Effect of pH

The initial pH of solution is expected to influence catalyst surface charge and hence the degradation of BPA. Therefore, the effect of pH in the range from 3 to 9 was investigated. A degradation of 73% was observed at pH 3, whereas when pH was increased to 7.5 (which was the natural pH of solution) the degradation of BPA increased to 99.5%. However, further increase in the pH led to decreased degradation from 99.5% to 69% at pH 9 (Fig. 8(b)).

The results are explained on basis of zero point charge (pH_{pzc}) of $ZG_{0.6}$ and pKa of BPA. The pH_{pzc} was found to be 7.0 using Malvern Zetasizer Nano ZS90 and shown in Fig. S2(b) (Supplementary information). On this basis, when pH<pH_{pzc}, the catalyst exists in cationic form, i.e., positively charged and if pH>pH_{pzc} catalyst exists in anionic form, i.e., negatively charged [34]. Moreover, the pKa of BPA is 9.6, which indicates that BPA molecules have positive charge between 7-9.6 [22]. The negative catalyst surface and positively charged BPA molecules exhibit electrostatic forces of attraction, hence resulting in high degradation of BPA at pH 7.5. However, in strongly alkaline condition (pH 9), nano-catalyst gets coagulated, resulting in decreased photocatalytic activity [34, 35]. The present study revealed that $ZG_{0.6}$ nanocatalyst has proficiency to degrade BPA under near to neutral conditions. It is a noteworthy outcome in comparison to the previous studies due to Bechambi et al. [22] and Hak et al. [20], who observed higher degradation at pH 8 and pH 3, respectively. It is pertinent to mention here that in case of studies due to Bechambi et al. [22] the pH_{pzc} of C-doped ZnO was 7.5, revealing negative charge on the catalyst surface above 7.5. Thus, higher degradation was observed in alkaline medium (pH 8) due to attraction between negatively charged surface and positively charged BPA molecules as observed in the present study. However, Hak et al. [20] worked on Au/C_3N_4 catalyst for the degradation of BPA and showed the highest catalytic activity in the highly acidic medium of pH 3.

2-5. Effect of Initial Concentration of BPA

Fig. 8(a) shows the effect of the initial concentration of BPA on its degradation. According to Gerhardt [7] and Yamamoto et al. [8], the concentration of BPA in water lies in the range of ~17-35 mg L^{-1}. Therefore, the concentration of BPA was varied in the range of 10 to 50 mg L^{-1}. Degradation increased with increase in irradiation time for a particular concentration of 10 mg L^{-1}. Typically, for a concentration of 20 mg L^{-1}, maximum degradation of 99.5% was observed after 60 min of UVC_{254} irradiation (Fig. 9(a)). A linear fit for ln(C_0/C) vs. irradiation time was observed for various BPA concentration. The linear plots with good correlation coefficients R^2>0.99 suggest that photocatalytic degradation followed pseudo-first-order kinetics. Further, the heterogeneous photocatalytic reaction was described by the Langmuir Hinshelwood (L-H) kinetic expression $\frac{1}{r_o}=\frac{1}{kKC_0}+\frac{1}{k}$ [36], where r_o is the initial rate of reaction (mg L^{-1} min^{-1}), C_0 is the initial concentration of BPA (mg L^{-1}), k is the reaction rate constant (mg L^{-1} min^{-1}) and K is the adsorption equilibrium constant (L mg^{-1}). Fig. 9(b) confirms the applicability of the Langmuir-Hinshelwood model. Values of k and K, calculated from the intercept and the slope of the straight line, are tabulated in Table 4. It was observed that the value of rate constant 'k' for $ZG_{0.6}$ was significantly higher in comparison to ZnO, $ZG_{0.3}$ and $ZG_{0.8}$ nanocatalysts, indicating better degradation using $ZG_{0.6}$ nano-catalyst.

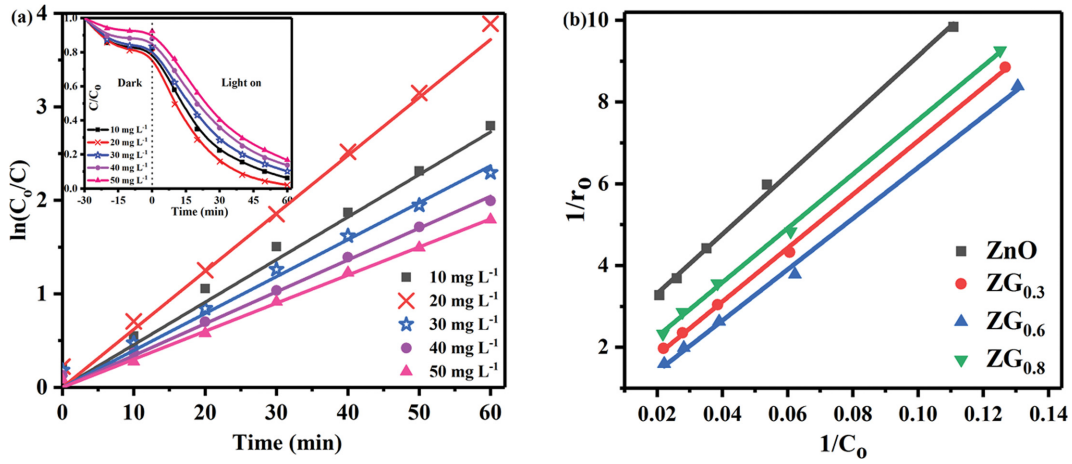


Fig. 9. Reaction kinetics and inset: change in BPA concentration versus irradiation time using $ZG_{0.6}$ (a); plot of inverse of rate of reaction ($1/r_o$) versus inverse of initial concentration ($1/C_0$) showed L-H relationship for ZnO, $ZG_{0.3}$, $ZG_{0.6}$ and $ZG_{0.8}$ (C_0=20 mg L^{-1}, catalyst dose 0.6 g L^{-1}, pH=7.5, UV intensity=15 W/m^2) (b).

Table 4. Parameters of Langmuir-Hinshelwood model

Catalyst	1/kK	1/k	k (mg L^{-1} min^{-1})	K (L mg^{-1})	R^2
ZnO	72.68	1.85	0.54	0.0254	0.99
$ZG_{0.3}$	62.40	0.15	2.04	0.0074	0.99
$ZG_{0.6}$	66.20	0.94	6.49	0.0025	0.99
$ZG_{0.8}$	65.56	0.49	1.07	0.0141	0.99

2-6. Mineralization Studies

In an ideal scenario BPA should finally decompose into simplest molecules like CO_2 and water. For this purpose, total organic carbon analysis was carried out using TOC analyzer. The reduction in value of total organic carbon (TOC) indicates the extent of mineralization. TOC values were recorded as a function of irradiation time using $ZG_{0.6}$ nanocatalysts for C_o: 20 mg L^{-1}, catalyst dose: 0.6 g L^{-1}, pH: 7.5, UV intensity: 15 W/m^2. TOC removal was found to be 90% after 120 min of irradiation (Fig. 10).

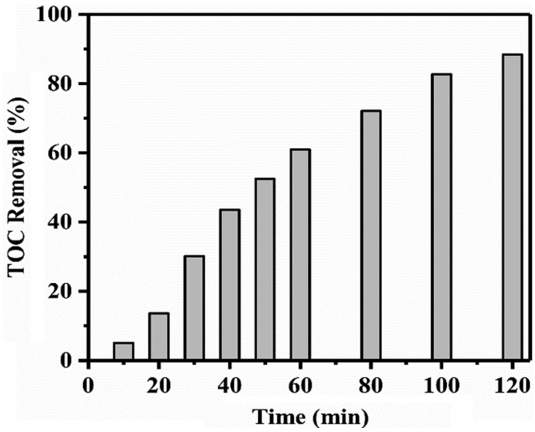


Fig. 10. TOC removal % of BPA using $ZG_{0.6}$ nano-catalyst at (C_o= 20 mg L^{-1}, catalyst dose 0.6 g L^{-1}, pH=7.5, UV intensity= 15 W/m^2).

2-7. Degradation Mechanism and Pathways

The degradation of BPA was monitored under ultraviolet light in the presence of $ZG_{0.6}$ catalyst. The proposed degradation pathways are in agreement with liquid chromatography-mass spectroscopy (LCMS) analysis (Fig. S2; Supplementary information). As per the reaction mechanism, ZnO nanocatalyst absorbed UV radiation to excite an electron from its valence band to conduction band, thus generating holes and electron charge carriers (Fig. 11). The generated electrons in the valence band of ZnO were transferred to conduction band of GO nanosheets (acting as electron collector) under UV-light irradiation, which further produced hydroxyl radicals (•OH). These radicals after striking BPA molecules resulted in oxidation/cleavage of some bonds in molecules and produced various fragments corresponding to m/z as shown by LCMS (Scheme 1). The details of the identified reaction intermediates along with their molecular formula, structure and mass error are compiled in Table 5. The intermediate product peaks appearing in the mass spectra of the available studies [4,6,10,22,37,38] are in good agreement with the present study. The mechanism involved the following reactions:

$$ZnO + h\nu \rightarrow ZnO(e^-_{cb}/h^+_{vb}) \rightarrow GO(e^-_{cb}) + h^+_{vb} \quad (3)$$

$$GO(e^-_{cb}) + O_2 \rightarrow O_2^{-}\bullet + H_2O \rightarrow \bullet OH \quad (4)$$

$$ZnO(h^+_{vb}) + H_2O \rightarrow \bullet OH + H^+ \quad (5)$$

$$\bullet OH + BPA \rightarrow Intermediates \rightarrow CO_2 + H_2O \quad (6)$$

In pathway I, BPA gets oxidized by •OH radicals and produces another compound 4-(1-(4-hydroxyphenyl)ethylidene)cyclohexa-2,5-dienone (1, m/z 212), which undergoes ring cleavage and produces compound (2, m/z 206). The compound 2, i.e., (E)-4-(4-hydroxyphenyl)-3-ethylpent-2-enoic acid, is oxidized to compound (3, m/z 196.1) by cleavage of C-C adjacent to ring and gave compound 4-(methylethenyl)phenol (4, m/z 134.1), which further produces fragments (10, 11, 12, 13) corresponding to m/z 154, 138, 110 and 94, respectively, by oxidation, which finally breaks into

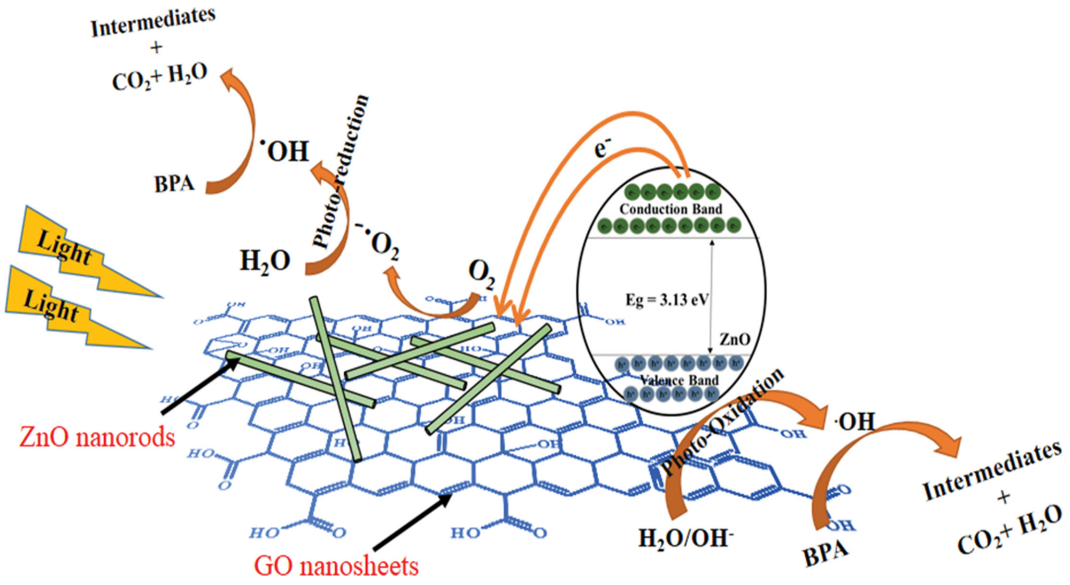
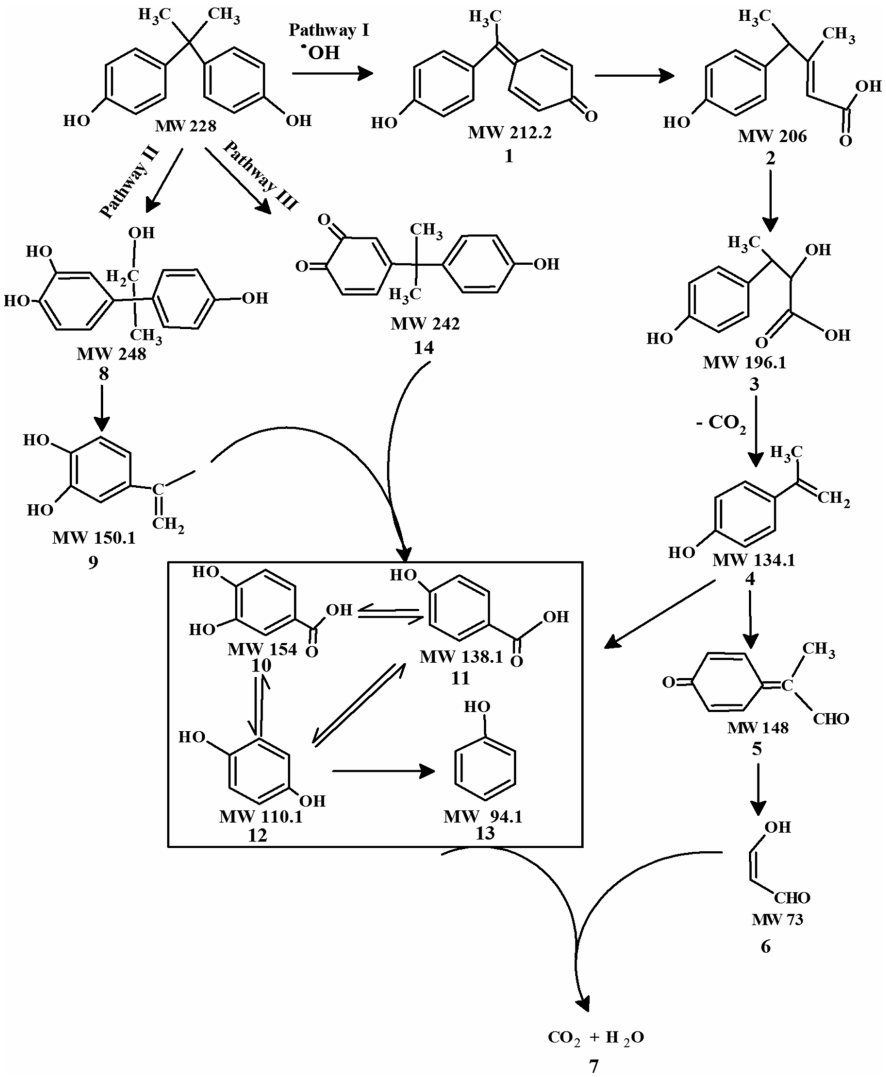
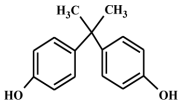
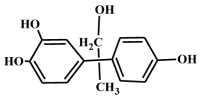
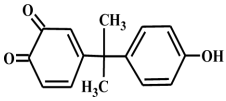
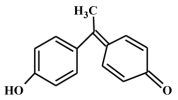
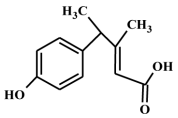
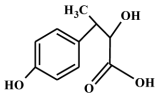
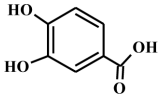
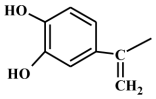
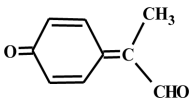
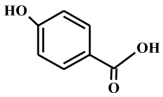
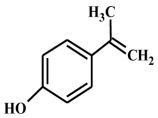
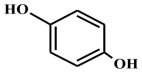
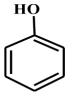


Fig. 11. Schematic representation of charge separation mechanism for degradation of BPA using $ZG_{0.6}$ nano-catalyst.



Scheme 1. Degradation Pathways for BPA using $ZG_{0.6}$ (C_o=20 mg L^{-1}, catalyst dose=0.6 g L^{-1}, pH=7.5, UV intensity=15 W/m^2).

Table 5. Details of reaction intermediates identified with chemical formula, structure and molecular weight for degraded Bisphenol A by mass spectra analysis

Intermediate name	Structure	MW (g/g mol)	Mass error	Similar peaks identified in literature
2,2-Bis(4-hydroxyphenyl)propane		228	-	[6,22]
2-(4-Hydroxyphenyl)-2-(3,4-dihydroxyphenyl)propanol		248	0.8	--
4-(2-(4-Hydroxyphenyl)propan-2-yl)cyclohexa-3,5-diene-1,2- dione		243	1.9	[4,6,37]
4-(1-(4-Hydroxyphenyl)ethylidene) cyclohexa-2,5-dienone		212.2	1.7	--
(E)-4-(4-Hydroxyphenyl)-3-methylpent-2-enoic acid		206	1.9	--
2-Hydroxy-3-(4-hydroxyphenyl)butanoic acid		196.1	2.8	--
3,4-Dihydroxybenzoic acid		154	1.1	[38]
4-(Prop-1-en-2-yl)benzene-1,2-diol		150	2.9	[37,38]
2-(4-Oxocyclohexa-2,5-dienylidene)propanol		148	0.1	--
4-Hydroxybenzoic acid		138.1	0.3	[38]
4-(Methylethenyl)phenol		134.1	0.0	[6,10,22]
Hydroquinol		110.1	0.6	[10,38]
Phenol		94.1	0.8	[22]
(Z)-3-Hydroxyacrylaldehyde		73	0.1	--

CO_2 and H_2O. The compound 4-(methylethenyl)phenol upon enolization gives compound (5, m/z 148), which is further oxidized by cleavage of ring to produce compound (6, m/z 73), which ultimately gives compound 7: CO_2 and H_2O.

Pathway II shows that aromatic rings are vulnerable to oxidation. The BPA molecule (m/z 228) undergoes hydroxylation in aromatic ring to form compound 2-(4-hydroxyphenyl)-2-(3,4-dihydroxyphenyl)propanol (8, m/z 248). Further, compound 8 produces compound (9, m/z 150) by cleavage of ring due to attack of $^{\bullet}OH$ radicals. Here the $-CH_3$ group oxidizes to alcohols so the rings of

BPA undergo oxidation by attack of radicals as well as -CH_3 group oxidizes to produce 3,4-dihydroxybenzoic acid (10, m/z 154), 4-hydroxybenzoic acid (11, m/z 138), hydroquinol (12, m/z 110) and phenol (13, m/z 94), which ultimately gives CO_2 and H_2O.

In pathway III, BPA might undergo oxidation to produce compound (14, m/z 243). Here two keto groups are present on one of aromatic ring. The various intense peaks in LCMS appear due to fragments (10, 11, 12, 13) corresponding to alcohol, aldehyde and carboxylic groups produced by oxidation in different ways. These fragments eventually mineralize to CO_2 and H_2O. Moreover, it is noteworthy that for the smaller byproducts the obtained peaks have higher intensity in comparison to the larger molecules.

2-8. Comparison with Literature Studies

Various studies on the degradation of BPA have been reported in the literature using different catalysts. Therefore, to evaluate the performance of $ZG_{0.6}$ nanocatalyst, a comparative study was conducted for the degradation efficiencies of different types of nanocatalysts available in the literature. Fig. 12 shows that the reported studies have lower degradation of BPA in comparison to the present study. However, Hak et al. [20] showed complete degradation of BPA using Au/g-C_3N_4 composite but it was achieved at highly acidic conditions (pH 3), whereas the present study has the clear advantage of degradation at near to neutral pH of 7.5.

2-9. Recyclability

To determine the efficiency of $ZG_{0.6}$ nanocatalyst the recyclability was studied for the five repeated runs. Herein, at the end of every experiment, catalyst was washed several times with de-ionized water and dried at 100±5 °C. Five repeated runs of the same catalyst were carried out consecutively and the percentage degradation of BPA was found to be 99.5%, 94.6%, 92.2%, 89.3%, and 87.1%, respectively (Fig. S3). The observed results had a fall of degradation from 99.5% to 87.1%. When the catalyst was reused four times, an activity of 87.1% after fourth reuse should be considered to be very good. Moreover, XRD analysis (Fig. 13(a)) and FESEM image (Fig. 13(b)) confirmed that the peaks as well as structure of nanocomposite were maintained even after fourth reuse. The slight loss in the catalytic activity of nanocatalyst might be due to the residual adsorption of BPA even after the washing.

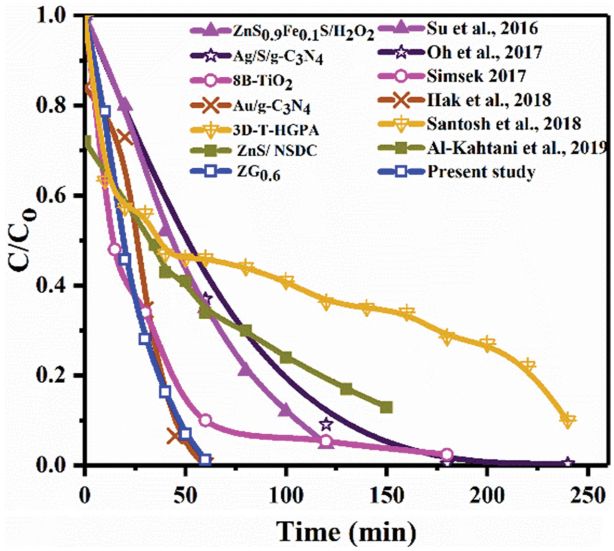


Fig. 12. Comparative study on BPA degradation using $ZG_{0.6}$ nanocatalyst.

CONCLUSION

This study investigated the photocatalytic degradation of an endocrine disrupter, BPA, in aqueous solutions using ZnO, GO, $ZG_{0.3}$, $ZG_{0.6}$, $ZG_{0.8}$ nanocatalysts under UV irradiations. The nanocatalyst $ZG_{0.6}$ was quite effective, in comparison to bare ZnO and GO nanocatalysts due to improved surface area and excellent separation of charge carriers. Interestingly, $ZG_{0.6}$ nanocatalyst showed highest degradation under its natural pH in a relatively short time of 60 min of irradiation with pseudo-first-order kinetics. 90% mineralization of BPA was possible after 120 min of UV irradiation. Based on LC-MS analysis, three different degradation pathways for BPA were proposed with formation of smaller by-products such as phenol, hydroquinol and (Z)-3-hydroxyacrylaldehyde, which were

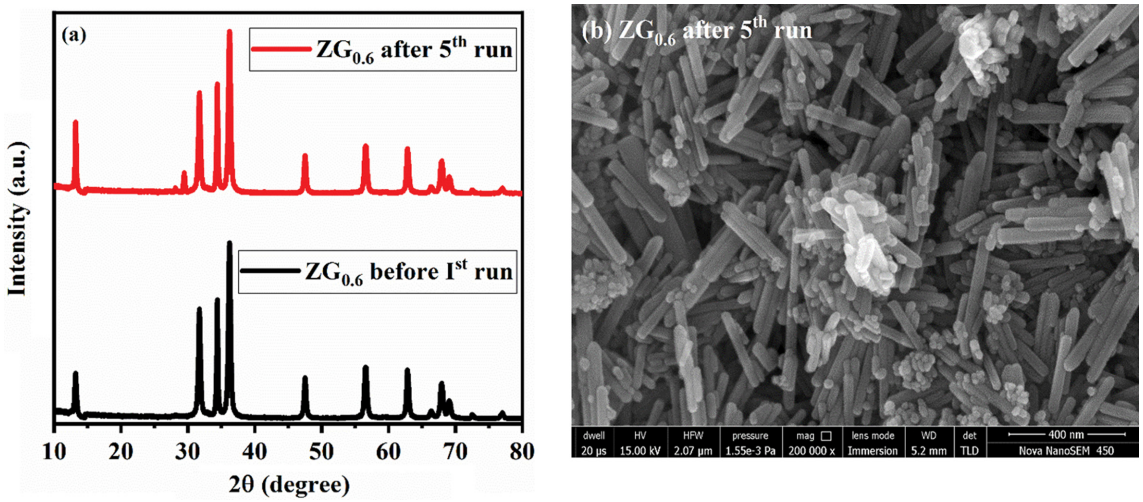


Fig. 13. Reusability study of $ZG_{0.6}$ nano-catalyst, XRD pattern (a); FESEM image after 4th reuse (b).

finally mineralized into CO_2 and H_2O. Overall, it can be concluded that $ZG_{0.6}$ is more effective and eco-friendly to degrade BPA from aqueous solutions in comparison to the literature studies.

ACKNOWLEDGEMENTS

Authors are thankful to MRC Malaviya National Institute of Technology Jaipur and SAIF Panjab University Chandigarh for assistance in analysis of sample. One of the authors, Ms. Renuka, is thankful to Ministry of Human Resource Development (MHRD), New Delhi for providing a fellowship.

SUPPORTING INFORMATION

Additional information as noted in the text. This information is available via the Internet at http://www.springer.com/chemistry/journal/11814.

REFERENCES

1. H. Katsumata, S. Kawabe, S. Kaneco, T. Suzuki and K. Ohta, *J. Photochem. Photobiol. A Chem.*, **162**, 297 (2004).
2. E. B. Simsek, *Appl. Catal. B, Environ.*, **200**, 309 (2017).
3. C. Santhosh, A. Malathi, E. Daneshvar, P. Kollu and A. Bhatnagar, *Sci. Rep.*, **8**, 15531 (2018).
4. W. H. M. Abdelraheem, M. K. Patil and M. N. Nadagouda, *Appl. Catal. B Environ.*, **241**, 598 (2019).
5. S. Flint, T. Markle, S. Thompson and E. Wallace, *J. Environ. Manage.*, **104**, 19 (2012).
6. V. Repousi, A. Petala, Z. Frontistis, M. Antonopoulou, I. Konstantinou, D. I. Kondarides and D. Mantzavinos, *Catal. Today*, **284**, 59 (2017).
7. A. Gerhardt, *J. Toxicol. Risk Assess.*, **5**, 17 (2019).
8. T. Yamamoto, A. Yasuhara, H. Shiraishi and O. Nakasugi, *Chemosphere*, **42**, 415 (2001).
9. H. Zhang, Y. Zhang, J. Li and M. Yang, *Sci. Total Environ.*, **655**, 607 (2019).
10. A. A. Al-Kahtani, S. M. Alshehri, M. Naushad, Ruksana and T. Ahamad, *Int. J. Biol. Macromol.*, **121**, 415 (2019).
11. EFSA, *EFSA J.*, **13**, 3978 (2015).
12. R. Atchudan, T. N. J. I. Edison, S. Perumal, M. Shanmugam and Y. R. Lee, *J. Photochem. Photobiol. A Chem.*, **337**, 100 (2017).
13. B. Jain, A. Hashmi, S. Sanwaria, A. K. Singh, M. A. B. H. Susan and A. Singh, *Adv. Compos. Hybrid Mater.*, **3**, 231 (2020).
14. V. N. Nguyen, D. Trinh, T. Manh and T. Nguyen, *Res. Chem. Intermed.*, **44**, 3081 (2018).
15. M. Maruthupandy, P. Qin and T. Muneeswaran, *Mater. Sci. Eng. B*, **254**, 114516 (2020).
16. Z. Durmus, B. Z. Kurt and A. Durmus, *ChemistrySelect*, **4**, 271 (2019).
17. T. Phatthanakittiphong and G. T. Seo, *Nanomaterials*, **6**, 128 (2016).
18. J. Xu, L. Wang and Y. Zhu, *Langmuir*, **28**, 8418 (2012).
19. M. Dükkancı, *Chem. Biochem. Eng. Q.*, **33**, 43 (2019).
20. C. H. Hak, L. C. Sim, K. H. Leong, Y. H. Chin and P. Saravanan, *IOP Conf. Ser. Mater. Sci. Eng.*, **409**, 012008 (2018).
21. M. Ozmen, A. Güngördü, S. Erdemoglu and N. Ozmen, *Aquat. Toxicol.*, **165**, 144 (2015).
22. O. Bechambi, S. Sayadi and W. Najjar, *J. Ind. Eng. Chem.*, **32**, 201 (2015).
23. D. C. Marcano, D. V Kosynkin, J. M. Berlin, A. Sinitskii, Z. Sun, A. Slesarev, L. B. Alemany, W. Lu and J. M. Tour, *ACS Nano*, **4**, 4806 (2010).
24. Y. Xu, J. Jin, X. Li, Y. Han, H. Meng, T. Wang and X. Zhang, *Mater. Res. Bull.*, **76**, 235 (2016).
25. R. Garg, R. Gupta and A. Bansal, *Int. J. Environ. Sci. Technol.*, In press (2020). https://doi.org/10.1007/s13762-020-02866-y.
26. P. S. Chauhan, R. Kant, A. Rai, A. Gupta and S. Bhattacharya, *Mater. Sci. Semicond. Process.*, **89**, 6 (2019).
27. K. Dai, L. Lu, C. Liang, J. Dai, G. Zhu, Z. Liu, Q. Liu and Y. Zhang, *Mater. Chem. Phys.*, **143**, 1410 (2014).
28. J. Qin, X. Zhang, Y. Xue, N. Kittiwattanothai, P. Kongsittikul, N. Rodthongkum, S. Limpanart, M. Ma and R. Liu, *Appl. Surf. Sci.*, **321**, 226 (2014).
29. Y. A. J. Al-hamadani, G. Lee, S. Kim, C. M. Park and M. Jang, *Chemosphere*, **205**, 719 (2018).
30. S. Archana, K. Y. Kumar, B. K. Jayanna, S. Olivera, A. Anand, M. K. Prashanth and H. B. Muralidhara, *J. Sci. Adv. Mater. Devices*, **3**, 167 (2018).
31. N. A. Rahmat, T. Hadibarata, A. Yuniarto, M. S. Elshikh and A. Syafiuddin, *IOP Conf. Ser. Mater. Sci. Eng.*, **495**, 012059 (2019).
32. A. Verma, A. P. Toor, N. T. Prakash, P. Bansal and V. K. Sangal, *New J. Chem.*, **41**, 6296 (2017).
33. R. Su, Y. Xue, G. Zhang, Q. Wang, L. Hu and P. Wang, *Photochem. Photobiol.*, **92**, 775 (2016).
34. N. Daneshvar, S. Aber, M.S. Seyed Dorraji, A. R. Khataee and M. H. Rasoulifard, *Sep. Purif. Technol.*, **58**, 91 (2007).
35. M. O. Fatehah, H. A. Aziz and S. Stoll, *J. Colloid Sci. Biotechnol.*, **3**, 75 (2014).
36. K. V. Kumar, K. Porkodi and F. Rocha, *Catal. Commun.*, **9**, 82 (2008).
37. W.-D. Oh, L.-W. Lok, A. Veksha, A. Giannis and T.-T. Lim, *Chem. Eng. J.*, **333**, 739 (2017).
38. C. Regmi, D. Dhakal and S. W. Lee, *Nanotechnology*, **29**, 64001 (2018).

Supporting Information

Degradation mechanism, reaction pathways and kinetics for the mineralization of Bisphenol A using hybrid ZnO/graphene oxide nano-catalysts

Renuka Garg, Renu Gupta, and Ajay Bansal[†]

Department of Chemical Engineering, Dr B R Ambedkar National Institute of Technology, Jalandhar, Punjab-144011, India
(*Received 9 July 2020 • Revised 17 November 2020 • Accepted 22 November 2020*)

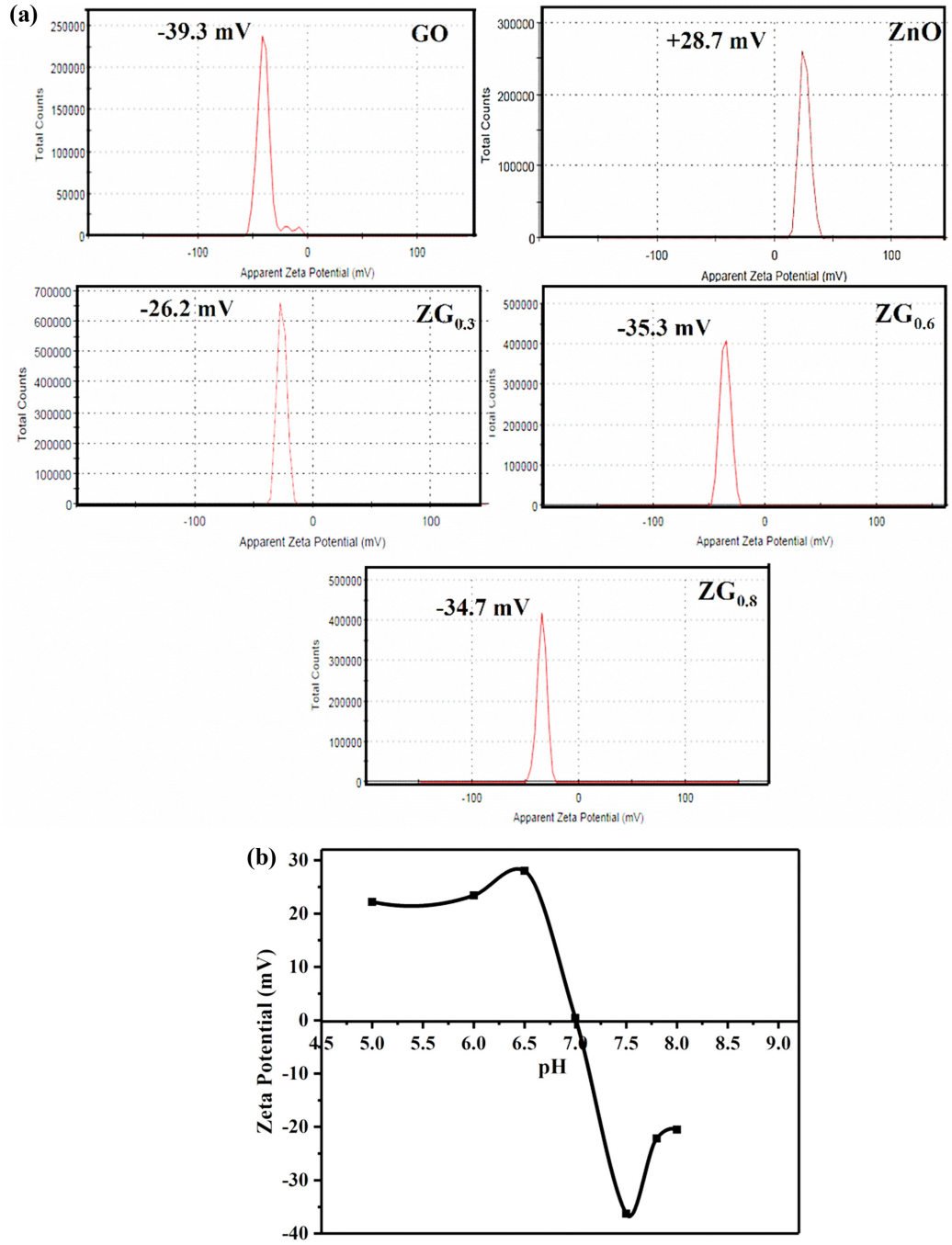


Fig. S1. Zeta potential at pH 7.5 for GO, ZnO, $ZG_{0.3}$, $ZG_{0.6}$ and $ZG_{0.8}$ nano-catalysts (a); point of zero charge at different pH (b).

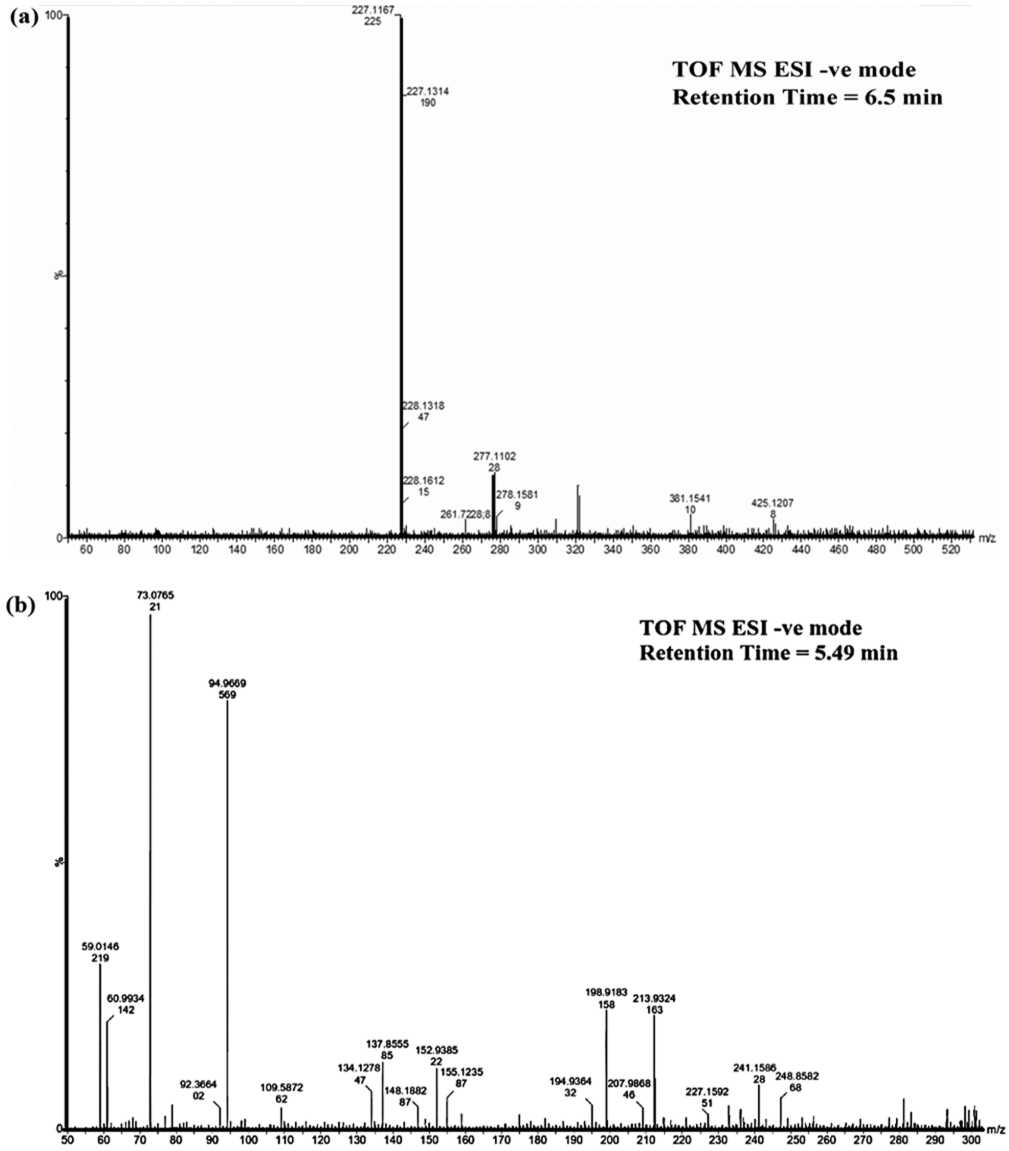


Fig. S2. Mass spectra before degradation (a); after degradation (b) of BPA (20 mg L^{-1}) using $ZG_{0.6}$ nano-catalyst at pH 7.5 under 60 min UV irradiation.

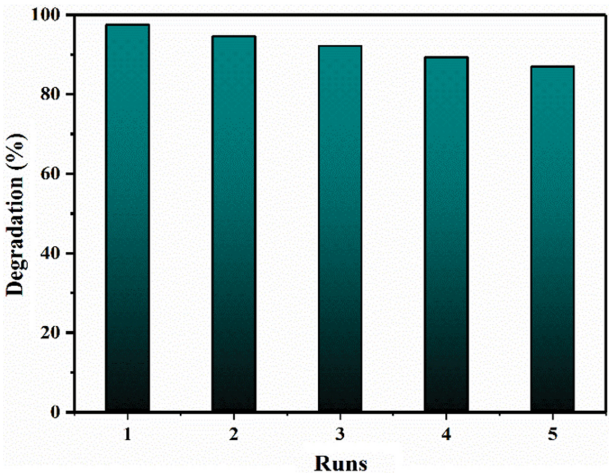


Fig. S3. Recyclability analysis of $ZG_{0.6}$ nano-catalyst for five runs.